Finite element analysis of stress distribution in porcelain discs

A. NAKATSUKA
Hiroshima Dental Technician School, 1-1 Sakatahonmachi, Hatsukaichi-shi, Hiroshima 738 Japan

K. J. ANUSAVICE
Department of Dental Biomaterials, College of Dentistry, University of Florida, Gainesville, FL 32610-0446 USA

Achievement of a controlled stress distribution in feldspathic porcelain is essential for successful dental restorations. In this study, a program for visco-elastic finite element analysis (FEM) of the stress distribution produced during processing of porcelain was developed. This method was applied to simulate the stress change in porcelain discs that were subjected to convective cooling. The heat transfer coefficient was assumed to be 2.1 $\mu J\ mm^{-2}\ min^{-1}\ °C^{-1}$ at the surface of the discs. These discs were 2 mm in thickness and had radii varying between 4.8 and 38 mm.

As the discs cooled from their sintering temperature, stresses initially developed at about 600 °C. Residual tensile stress of 8.3 MPa was produced at the centre of the top surface of a 16-mm diameter disc compared with a compressive stress of -7.6 MPa for a 50-mm diameter disc.

1. Introduction

Porcelain has been used in the dental field as an important material. One of the potential problems of this material is its susceptibility to fracture caused by thermal stresses that are introduced during the cooling process following a sintering heat treatment at temperatures between 800 and 1000 °C. Large temperature gradients in the porcelain may result in instantaneous fracture during cooling. Recent studies have shown that even if the transient tensile stress during cooling is not large enough to cause instantaneous failure, it can cause delayed crack initiation in porcelain that can result in fracture at a later time. This "delayed failure" can occur after months or years [1]. On the other hand, it is possible to strengthen dental porcelain by introducing compressive stress within its surface by means of forced convective cooling in air [2]. Therefore, it is important to analyse the stress distribution in porcelain models in order to optimize the processing conditions for fabrication of porcelain prostheses.

Visco-elastic analysis is necessary to determine the distribution of stresses in fired porcelains because the porcelain is expected to be in a visco-elastic state near its glass transition temperature. This analysis takes into consideration the stress relaxation that occurs over a certain temperature range, and it represents a more reliable method for estimation of stress values than elastic analysis [3]. DeHoff and Anusavice analysed stress distributions in porcelain discs and strips using the visco-elastic theory of Narayanaswamy [4–6]. Asaoka and Tesk used the Voigt model in a multi-plate model to analyse stresses in a porcelain-metal strip [7]. However, these applications of visco-elastic analyses have been limited to simple geometries such as bimaterial strips or discs. Thus, it is necessary to develop an analytical model available for more practical conditions because dental crowns are associated with more complex shapes and temperature distributions. The finite element method (FEM) represents an effective approach to analyse stress distributions in these practical conditions. A computer program for FEM analysis was developed in which each element of the model can have unique value of viscosity and thermal contraction coefficient according to the temperature distributions.

The objective of this study was to analyse the influence of the disc dimensions on stress distributions predicted by FEM calculations.

2. Materials and methods

Thermal contraction and viscosity were measured for Biobond opaque porcelain (Dentsply International, York, PA).

2.1. Measurement of thermal contraction

Specimens were prepared as $5 \times 5 \times 50.8$ mm bars according to the manufacturer's recommendation.

0022–2461

Values of $\Delta L/L$ were calculated from contraction data determined according to ASTM Standard E228-71 using an Orton dilatometer (Orton Ceramic Foundation, Columbia, OH). The contraction of each specimen was measured over the range of 600 to 25 °C at a cooling rate of approximately 3 °C min^{-1}. Thermal contraction values were calculated at 25 °C intervals.

2.2. Measurement of creep rate

The shear viscosity of porcelain was calculated from creep rates measured in a beam-bending viscometer using the following equation [5, 8]

$$\eta = \frac{L^3}{144\,VI_C}P + \frac{\rho g w d L}{1.6} \quad (1)$$

where I_C is the cross-section moment of inertia (m^4), η is the shear viscosity (N s m^{-1}), V is the midpoint deflection rate (m s^{-1}), P is the midspan load (N), ρ is the density (kg m^{-3}), g is the acceleration of gravity (m s^{-2}), w is the specimen width (m), and d is the specimen height (m). In this study, L and P were 47 mm and 9.8 N, respectively. A specimen strip, $2.4 \times 5.8 \times 57$ mm, was prepared according to the schedule recommended by the porcelain manufacturer. The temperature was raised from 450 to 625 °C at a rate of 3 °C min^{-1}, and the temperature was held constant at 25 °C intervals to obtain the creep rate at each temperature.

2.3. General method of visco-elastic analysis by FEM

The Maxwell model and the Voigt model have been used traditionally to analyse developing stresses in visco-elastic materials although neither model is precise enough to simulate the actual visco-elastic behaviour. Both models consist of two elements (spring and dashpot). These elements are connected in series for the Maxwell model and in parallel for the Voigt model. Porcelain is expected to deform freely under constant tensile stress in a glassy state. Since the Voigt model cannot represent the creep behaviour of porcelain, only the Maxwell model was employed in this study.

According to the Maxwell model for a one-dimensional problem, the constitutive relation between stress and strain is

$$\frac{d\varepsilon}{dt} = \frac{1}{E}\frac{d\sigma}{dt} + \frac{\sigma}{\eta} \quad (2)$$

where E is the Young's modulus and η is the viscosity. By introducing finite time increments Δt_i and thermal strain $\alpha_i \Delta T_i$, Equation 2 becomes

$$\Delta\varepsilon_i = \frac{1}{E}\Delta\sigma_i + \frac{\sigma_i}{\eta_i}\Delta t_i + \alpha_i \Delta T_i \quad (3)$$

or

$$\Delta\sigma_i = E\left(\Delta\varepsilon_i - \frac{\sigma_i}{\eta_i}\Delta t_i - \alpha_i \Delta T_i\right) \quad (4)$$

where η_i is the viscosity, α_i is the thermal contraction coefficient at the middle of time step i, and ΔT_i, is the temperature change in time step i. Equation 3 shows that the strain change during Δt_i consists of three terms: (1) elastic strain, (2) viscous strain, and (3) thermal strain.

For two- or three-dimensional visco-elastic problems of isotropic materials, it is necessary to determine shear and bulk creep compliances. Maxwell models were assumed for both shear and bulk compliances in this study. Viscous behaviour was characterized by shear viscosity η_{Ki} and bulk viscosity η_{Gi}, and relations between stress and viscous strain change become Equation 5 by analogy with the elastic theory [9, 10]

$$\begin{pmatrix} \Delta\varepsilon_{xx} - \Delta\varepsilon_m \\ \Delta\varepsilon_{yy} - \Delta\varepsilon_m \\ \Delta\varepsilon_{zz} - \Delta\varepsilon_m \\ \Delta\varepsilon_{xy} \\ \Delta\varepsilon_{yz} \\ \Delta\varepsilon_{zx} \end{pmatrix}_i = \frac{\Delta t_i}{2\eta_{Gi}} \begin{pmatrix} \sigma_{xx} - \sigma_m \\ \sigma_{yy} - \sigma_m \\ \sigma_{zz} - \sigma_m \\ \tau_{xy} \\ \tau_{yz} \\ \tau_{zx} \end{pmatrix}_i$$

$$\begin{pmatrix} \Delta\varepsilon_m \\ \Delta\varepsilon_m \\ \Delta\varepsilon_m \\ 0 \\ 0 \\ 0 \end{pmatrix}_i = \frac{\Delta t_i}{3\eta_{Ki}} \begin{pmatrix} \sigma_m \\ \sigma_m \\ \sigma_m \\ 0 \\ 0 \\ 0 \end{pmatrix}_i \quad (5)$$

where σ_m is the mean stress, $\sigma_m = (\sigma_{xx} + \sigma_{yy} + \sigma_{zz})/3$, and ε_m is the mean strain, $\varepsilon_m = (\varepsilon_{xx} + \varepsilon_{yy} + \varepsilon_{zz})/3$ and τ is the shear stress. Equation 6 is derived from Equation 5

$$\begin{pmatrix} \Delta\varepsilon_{xx} \\ \Delta\varepsilon_{yy} \\ \Delta\varepsilon_{zz} \\ \Delta\varepsilon_{xy} \\ \Delta\varepsilon_{yz} \\ \Delta\varepsilon_{zx} \end{pmatrix}_i = \frac{\Delta t_i}{18\eta_{Gi}\eta_{Ki}} \begin{pmatrix} 2\eta_{Gi} + 6\eta_{Ki} & 2\eta_{Gi} - 3\eta_{Ki} & 2\eta_{Gi} - 3\eta_{Ki} & 0 & 0 & 0 \\ 2\eta_{Gi} - 3\eta_{Ki} & 2\eta_{Gi} + 6\eta_{Ki} & 2\eta_{Gi} - 3\eta_{Ki} & 0 & 0 & 0 \\ 2\eta_{Gi} - 3\eta_{Ki} & 2\eta_{Gi} - 3\eta_{Ki} & 2\eta_{Gi} + 6\eta_{Ki} & 0 & 0 & 0 \\ 0 & 0 & 0 & 9\eta_{Ki} & 0 & 0 \\ 0 & 0 & 0 & 0 & 9\eta_{Ki} & 0 \\ 0 & 0 & 0 & 0 & 0 & 9\eta_{Ki} \end{pmatrix} \begin{pmatrix} \sigma_{xx} \\ \sigma_{yy} \\ \sigma_{zz} \\ \tau_{xy} \\ \tau_{yz} \\ \tau_{zx} \end{pmatrix}_i \quad (6)$$

If it is assumed that no change in volume occurs during viscous deformation, η_K is considered to be ∞. Then, Equation 6 becomes

$$\begin{pmatrix} \Delta\varepsilon_{xx} \\ \Delta\varepsilon_{yy} \\ \Delta\varepsilon_{zz} \\ \Delta\varepsilon_{xy} \\ \Delta\varepsilon_{yz} \\ \Delta\varepsilon_{zx} \end{pmatrix}_i = \frac{\Delta t_i}{6\eta_{Gi}} \begin{pmatrix} 2 & -1 & -1 & 0 & 0 & 0 \\ -1 & 2 & -1 & 0 & 0 & 0 \\ -1 & -1 & 2 & 0 & 0 & 0 \\ 0 & 0 & 0 & 3 & 0 & 0 \\ 0 & 0 & 0 & 0 & 3 & 0 \\ 0 & 0 & 0 & 0 & 0 & 3 \end{pmatrix} \begin{pmatrix} \sigma_{xx} \\ \sigma_{yy} \\ \sigma_{zz} \\ \tau_{xy} \\ \tau_{yz} \\ \tau_{zx} \end{pmatrix}_i \quad (7)$$

Considering that the total strain change consists of elastic, viscous, and thermal strain, the following relation can be obtained as a constitutive relation between stress and strain, instead of Equation 2

$$(\Delta\varepsilon)_i = (D)\,(\Delta\sigma)_i + (V)_i(\sigma)_i + \alpha_i\,\Delta T_i \quad (8)$$

where

$$(\Delta\varepsilon)_i = \begin{pmatrix} \Delta\varepsilon_{xx} \\ \Delta\varepsilon_{yy} \\ \Delta\varepsilon_{zz} \\ \Delta\varepsilon_{xy} \\ \Delta\varepsilon_{yz} \\ \Delta\varepsilon_{zx} \end{pmatrix}_i \quad (\Delta\sigma)_i = \begin{pmatrix} \Delta\sigma_{xx} \\ \Delta\sigma_{yy} \\ \Delta\sigma_{zz} \\ \Delta\tau_{xy} \\ \Delta\tau_{yz} \\ \Delta\tau_{zx} \end{pmatrix}_i$$

$$(\sigma)_i = \begin{pmatrix} \sigma_{xx} \\ \sigma_{yy} \\ \sigma_{zz} \\ \tau_{xy} \\ \tau_{yz} \\ \tau_{zx} \end{pmatrix}_i \quad (eT)_i = \alpha_i \begin{pmatrix} \Delta T_i \\ \Delta T_i \\ \Delta T_i \\ 0 \\ 0 \\ 0 \end{pmatrix}$$

and

$$(V)_i = \frac{\Delta t_i}{6\eta_{Gi}} \begin{pmatrix} 2 & -1 & -1 & 0 & 0 & 0 \\ -1 & 2 & -1 & 0 & 0 & 0 \\ -1 & -1 & 2 & 0 & 0 & 0 \\ 0 & 0 & 0 & 3 & 0 & 0 \\ 0 & 0 & 0 & 0 & 3 & 0 \\ 0 & 0 & 0 & 0 & 0 & 3 \end{pmatrix}$$

and (D) is the usual matrix used in elastic FEM calculations.

For the three-dimensional model, Equation 4 becomes

$$(\Delta\sigma)_i = (D)\,(\Delta\varepsilon)_i - (D)\,[(V)_i\,(\sigma)_i + (eT)_i] \quad (9)$$

These equations indicate that the visco-elastic problem for each time step is identical to the elastic problem except that the thermal strain term is $[(V)_i\,(\sigma)_i + (eT)_i]$ for visco-elastic behaviour, and $(eT)_i$ for elastic behaviour. Then, the elemental equations for the visco-elastic problem become

$$(K)\,(\Delta u)_i = \text{vol}\,(B)^T(D)\,[(V)_i\,(\sigma)_i + (eT)_i] + (\Delta f)_i$$
$$(K) = \text{vol}\,(B)^T(D)(B) \quad (10)$$

where (B) is the same matrix used in the FEM calculation for elastic problems, $(\Delta u)_i$ and $(\Delta f)_i$ are changes of displacement and external force for step i, respectively, and vol is the volume of the element.

To improve the accuracy, $[(\sigma)_i + (\sigma)_{i+1}]/2$ was used instead of $(\sigma)_i$ in Equations 9 and 10 in this study. Then, Equations 9 and 10 can be transformed into Equations 11 and 12, respectively

$$(\Delta\sigma)_i = (\sigma)_{i+1} - (\sigma)_i$$
$$= (D)(B)(\Delta u)_i - (D)(V)_i \times [(\sigma)_i + (\sigma)_{i+1}]/2 + (eT)_i \quad (11)$$

$$(K)\,(\Delta u)_i = \text{vol}\,(B)^T(D)\,\{(V)_i\,[(\sigma)_i + (\sigma)_{i+1}]/2 + (eT)_i\} + (\Delta f)_i \quad (12)$$

Equation 13 was obtained from Equation 11

$$(\Delta\sigma)_i = (\sigma)_{i+1} - (\sigma)_i$$
$$= (D_0)_i(B)(\Delta u)_i - (D_0)_i(V)_i(\sigma)_i - (D_0)_i(eT)_i \quad (13)$$

where $(D_0)_i = [(D)^{-1} + (V)_i/2]^{-1}$.

Using Equation 13, and the relation $(D)\,(V)_i = (V)_i(D)$, which can be obtained by direct calculation, Equation 12 becomes

$$\text{vol}(B)^T(D_0)_i(B)(\Delta u)_i = \text{vol}\,(B)^T(D_0)_i\,[(V)_i(\sigma)_i + (eT)_i] + (\Delta f)_i \quad (14)$$

Equations 13 and 14 are the final equations to be solved. Equations for the axisymmetric problem were obtained in the same manner as that used for the elastic situation for analyses of stress distributions in porcelain discs.

2.4. Process of calculations

First, the time was divided into SN steps (the total number of short time steps) and calculation at each step i was made as follows:

2.4.1. Calculation of temperature

Prior to calculations of stresses, the temperature history was analysed by a commercial FEM program (Nikkan Kougyo Shinbunsha, Tokyo, Japan). The temperature of each element at the middle of step i, T_i was determined as the average value of temperatures at three nodes of the element.

2.4.2. Calculations of viscosity and thermal contraction coefficient

Since viscosity is dependent on temperature, an Arrhenius relation, $\eta_G = \eta_0 \exp(B/T)$, was assumed, where η_0 and B are constants, and T is absolute temperature. Then, the viscosity of each element at time step i, η_i, becomes $\eta_{Gi} = \eta_0 \exp(B/T_i)$.

The thermal contraction coefficient of each element at the middle of step i, α_i, was determined using the following linear relations

$$\begin{aligned} \alpha_i &= A + B\,T_i \quad (T_i \leqslant T_g) \\ \alpha_i &= C(T_i - T_g) + A + B\,T_g \quad (T_i > T_g) \end{aligned} \tag{15}$$

where A, B and C, are constants and T_g is the glass transition temperature. These values were determined from measurements of thermal contraction. It has been reported that glass transition temperature depends on cooling rate [11]. Dependence of T_g on the cooling rate q was calculated by following Moynihan's equation [12]

$$\frac{d[\ln(q)]}{dT(1/T_g)} = -B \tag{16}$$

2.4.3. Calculations of displacement and stress change

Displacement of each node was determined by solving Equation 14 under appropriate boundary conditions.

The stress change of each element during this step was calculated using Equation 13 from the calculated displacements. Then, stress values, which were necessary for calculation at the next step, $i + 1$, were determined by $(\sigma)_{i+1} = (\Delta\sigma)_i + (\sigma)_i$. If $i < SN$, the process was repeated until i became equal to SN. All calculations were made on a PC-9801VM microcomputer (NEC Co., Japan).

2.5. Application of FEM calculation for discs

2.5.1. FEM models for analyses

Fig. 1 shows analysed models considering rotational symmetry. Discs had the same thickness of 2.0 mm, but their radii were 4.8, 8.0, 12.0, 16.3, 25.0 and 38.0 mm.

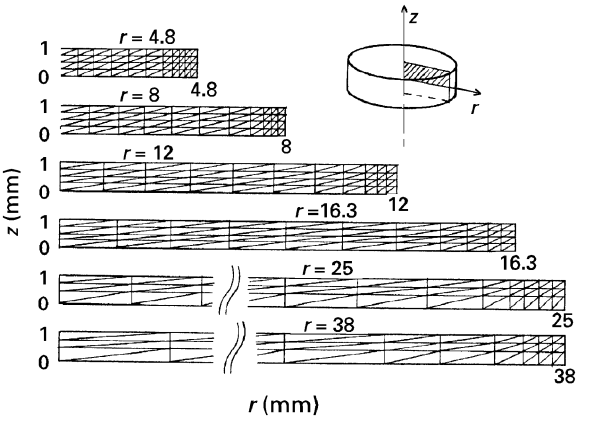

Figure 1 FEM models of discs.

2.5.2. Conditions for temperature analyses

Temperature history in the disc was analysed by FEM under the following conditions:

1. The thermal conductivity of the porcelain was 6.3×10^{-2} J mm^{-1} min^{-1} °C^{-1}.
2. The specific heat of the porcelain was 8.4×10^{-2} J mm^{-1} min^{-1} and the density was 24.5×10^{-6} N mm^{-3}.
3. The coefficient of heat transfer was $h = 2.1$ μJ mm^{-2} min^{-1} °C^{-1} at the top and side surfaces of the disc, and $h = 0$ J mm^{-2} min^{-1} °C^{-1} at the central axis and midplane of the disc. For a control model that represents a large porcelain plate, $h = 0$ J mm^{-2} min^{-1} °C^{-1} at the side surface as well as the central axis and midplane of the disc ($r = 8$ mm).
4. The initial temperature of 800 °C was distributed uniformly throughout the disc. Time was divided into 30 steps, and temperature history was calculated through 5 min from the start of cooling.
5. The environmental temperature was 20 °C.

2.5.3. Conditions for stress analyses

Stresses in the discs were calculated by the method described above.

Displacements were zero at the central axis in the radial direction and zero at the midplane in the direction of thickness. In this study $SN = 10$ and calculations were made from 0.01 min after the start of cooling through 3 min. The mechanical properties used in calculations are listed in Table I.

3. Results and discussion

3.1. Thermal contraction coefficient and viscosity of the porcelain

Fig. 2 shows that the relation between thermal contraction coefficient and temperature can be approximated by two linear relations. Coefficients, A, B and C in Equation 12 were obtained by the method of least squares and are listed in Table I. The intersection of these two lines, representing the glass transition point, occurred at 503 °C.

3.2. Viscosity of the porcelain

Fig. 3 shows the relationship between creep viscosity and the inverse of temperature. The following constants were obtained for the equation, $\eta = \eta_0 \exp(B/T)$: $\eta_0 = 9.6 \times 10^{-10}$ Pa/s and $B = 43\,218(1/K)$.

TABLE I Mechanical properties used in calculations

Thermal contraction coefficients
$\alpha = A + B\,T \quad (T \leqslant T_g)$
$\alpha = C(T - T_g) + A + B\,T_g \quad (T > T_g)$
$A = 1.08 \times 10^{-5}$, $B = 1.66 \times 10^{-8}$, $C = 6.33 \times 10^{-8}$, $T_g = 503$ °C
Viscosity $\eta = \eta_0 \exp(B/T)$
$\eta_0 = 9.6 \times 10^{-10}$ Pa/s, $B = 43\,218$ (1/K)
Young's modulus $E = 80$ GPa
Poisson's ratio $\nu = 0.2$

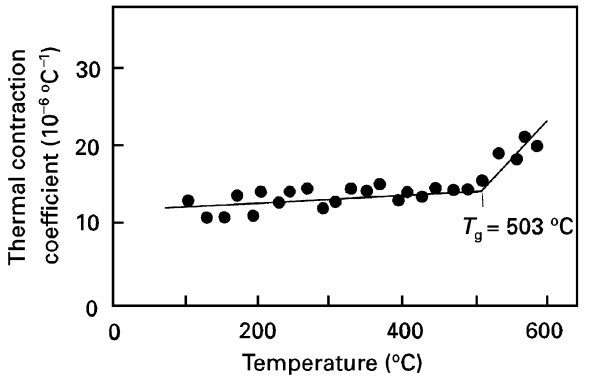

Figure 2 Relationship between thermal contraction coefficient and temperature.

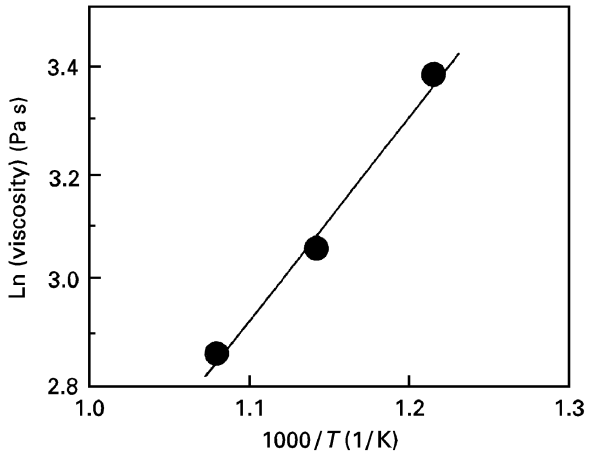

Figure 3 Relationship between viscosity and reciprocal temperature.

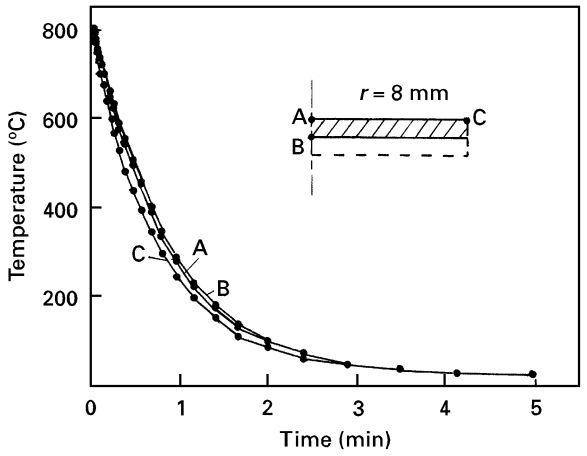

Figure 4 Temperature history in 16-mm diameter disc determined by FEM.

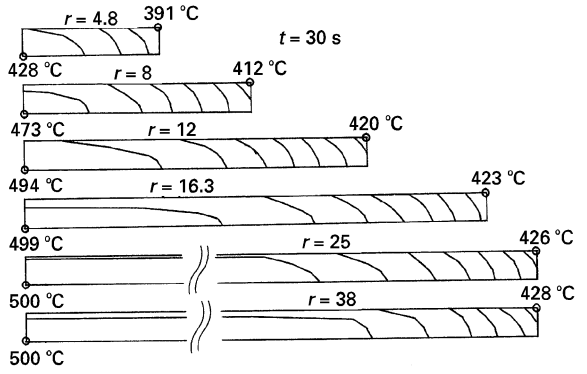

Figure 5 Temperature distribution in discs 30 s after the start of cooling from 800 °C determined by FEM.

3.3. Temperature history of discs

Fig. 4 shows the calculated temperature for a 16-mm diameter disc at the centre of the top surface (A), at the edge of the top surface (B), and at the centre of the midplane (C). The maximum temperature difference between point C and point B was about 60 °C, and that between point B and point A was about 5 °C.

Fig. 5 shows the temperature distribution in discs 30 s after the start of cooling. For each disc, the maximum temperature was found at A, and the minimum temperature at C. Temperature gradients exist mainly in the direction of thickness near the centre of each disc, especially when the radius is greater than 12 mm. The temperature gradient in the radial direction was found near the side surface of the disc.

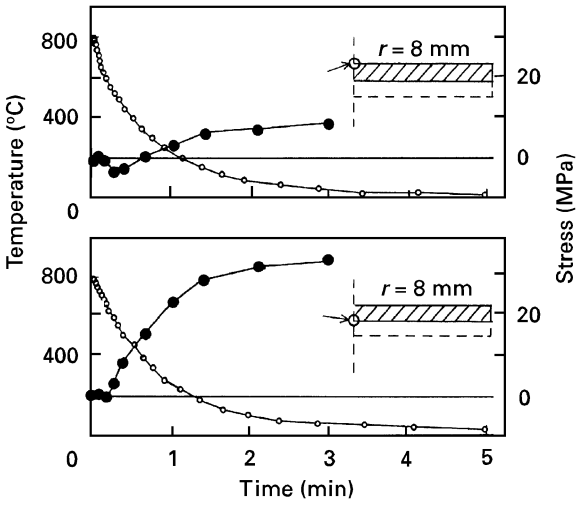

Figure 6 Stress and temperature histories in a disc with 8 mm radius. (●) Stress; (○) temperature.

3.4. Stress distribution in discs

All stresses in this report are radial component values. Fig. 6 shows stress and temperature changes at the centre of the top surface and at the centre of the midplane over time for $r = 8$ mm. Stresses began to increase at about 600 °C at both points. Above this temperature, stress relaxation occurs quickly enough not to introduce tangential stress in porcelain.

Stress distributions at the top surface along the radial direction are shown in Fig. 7. Stresses at the centre of the top surface were compressive for discs with radii of 16 mm, 25 mm and 38 mm. Stresses at the centre of the top surface were tensile for discs with radii of 4.8 mm, 8 mm, and 12 mm (Fig. 8).

These results indicate that porcelain discs that are cooled at an h value of 2.1 μJ mm^{-2} min^{-1} °C^{-1} can have a smaller strength than those that were cooled

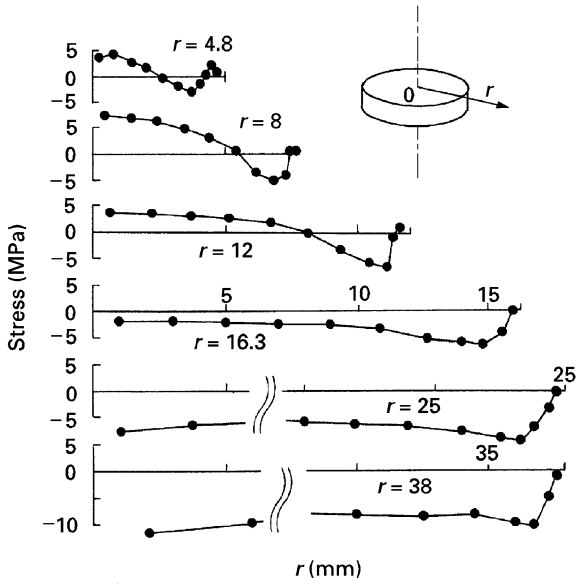

Figure 7 Stress distributions along the radial direction at the top surface.

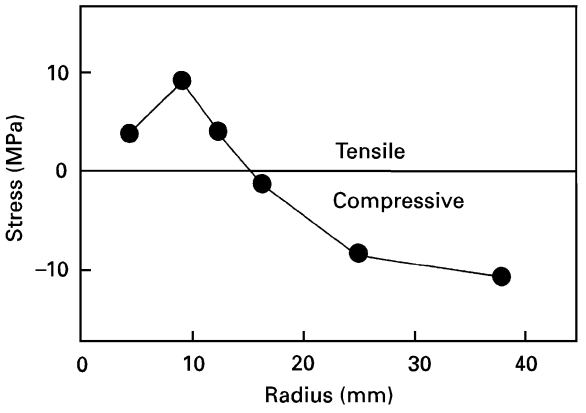

Figure 8 Relation between radius of disc and stress at the centre of the top surface.

slowly enough so that no residual stress was introduced when the radius of disc is less than 12 mm. Tensile stress at the surface enhances crack growth and decreases the strength of porcelain [2].

Stress distributions along the central axis of the discs are shown in Fig. 9. All profiles are parabolic; however stress values shifted toward negative values when the disc radius increased except for a radius of 4.8 mm. Stress distributions along the thickness in a porcelain strip have been reported previously. DeHoff and Anusavice used the theory of Narayanaswamy [5], and Asaoka and Tesk used a Voigt model to analyse stresses in a slab by the multi-strip model [7]. However, both of these studies neglected the effect of temperature gradient in the radial direction. Their condition corresponds to the control model in which $r = 8$ mm and the heat convection coefficient is 0 J mm^{-2} min^{-1} °C^{-1} at the side surface of the disc. Fig. 10 shows the stress distribution for the control model. These results for the control model agreed well with those reported previously [5, 7].

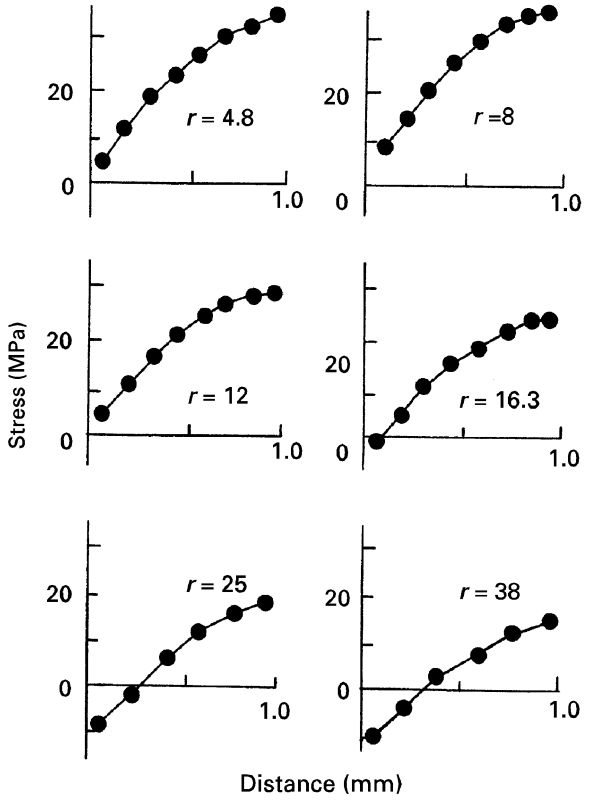

Figure 9 Stress distribution along the central axis.

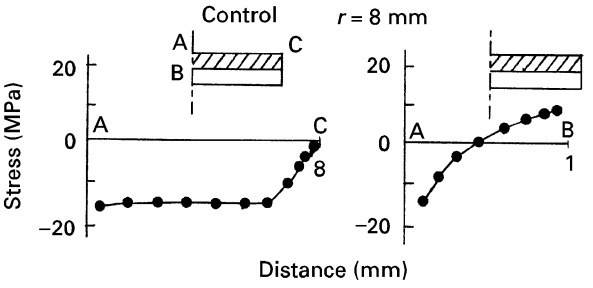

Figure 10 Stress distribution in control model for a heat transfer coefficient of zero at the side wall of the disc as well as the midplane location.

These results can be explained as follows. When discs are subjected to convective cooling, the side surface of the disc becomes cool and stiff at first. This stiff ring restricts thermal contraction of the inner part of the porcelain. This restriction introduces tensile stresses into the internal region. According to the theory of elasticity, the relation between pressure and displacement for an elastic ring is given by the following expression

$$U = \frac{(1-\nu)}{E}\frac{(A^2 P_i - B^2 P_o)}{(B^2 - A^2)} r + \frac{(1+\nu)}{E}\frac{A^2 B^2 (P_i - P_o)}{(B^2 - A^2)}\frac{1}{r} \quad (17)$$

where E is Young's modulus, ν is Poisson's ratio, A is the internal radius, B is the external radius, P_o is the external pressure, P_i is the internal pressure, r is the distance from the centre of the ring, and U is the

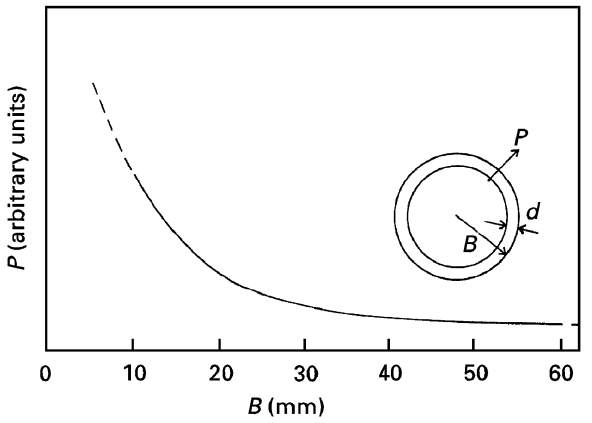

Figure 11 Elastic simulation of the relationship between the radius and stress at the centre of the top surface (Equation 19). $d = 3$ mm.

displacement at a distance from the centre. Considering the $P_o = 0$, the following equation can be derived from Equation 17

$$U(\text{at } r = B - d) = (B - d)\alpha\Delta T = \frac{P(B-d)}{E}\frac{[(1-\nu)(B-d)^2 + (1+\nu)B^2]}{B^2 - (B-d)^2} \quad (18)$$

where $d = B - A$. When $\alpha\Delta T$ is constant, Equation 18 becomes Equation 19

$$P = \text{constant} \Big/ \left[\frac{2 - 2(d/B) + (d/B)^2}{2(d/B) - (d/B)^2} + \nu\right] \quad (19)$$

The relationship between P and B is shown in Fig. 11, where ν and d are assumed to be 0.3 and 3 mm, respectively, for the stiff ring formed at the edges of discs during the cooling process. This profile is virtually equivalent to that for the relationship between stress at the centre of the top surface and the specimen radius shown in Fig. 8. Thus, it is suggested that the effect of the temperature gradient in the radial direction on the stress value at the centre of the disc still remains when the radius of the disc is 38 mm.

This study shows that the calculation method used in this study provides reasonable results. Comparisons between calculations and experimental data should enhance our understanding of the visco-elastic behaviour of dental porcelain in the future.

References

1. K. J. ANUSAVICE, A. GRAY and C. SHEN, *J. Dent. Res.* **70** (1991) 131.
2. K. J. ANUSAVICE, P. H. DEHOFF, B. HOJJATIE and A. GRAY, *ibid.* **68** (1989) 1182.
3. R. L. BERTOLOTTI, *ibid.* **59** (1980) 1972.
4. P. H. DEHOFF and K. J. ANUSAVICE, *ibid.* **71** (1992) 1139.
5. *Idem., ibid.* **68** (1989) 134.
6. O. S. NARAYANASWAMY, *J. Amer. Ceram. Soc.* **54** (1971) 491.
7. K. ASAOKA and J. A. TESK, *Dent. Mater. J.* **8** (1989) 9.
8. P. H. DEHOFF and K. J. ANUSAVICE, *J. Dent. Res.* **65** (1986) 643.
9. Y. YAMADA and K. IWATA, *Seisan-Kenkyu* **24** (1972) 165.
10. Y. YAMADA, in "Plasticity and visco-elasticity" (Baifukan Co., Tokyo, 1991) p. 124 (in Japanese).
11. K. ASAOKA, M. KON and N. KUWAYAMA, *Dent. Mater. J.* **9** (1990) 193.
12. C. T. MOYNIHAN, A. J. EASTEAL and J. WILDER, *J. Phys. Chem.* **78** (1974) 2673.

Received 6 February 1995
and accepted 13 November 1996